Evaluating radial component current measurements from CODAR high frequency radars and moored in situ current meters

Brian M. Emery[1], Libe Washburn[1,2], and Jack A. Harlan[3]

[1]*Institute for Computational Earth System Science, University of California, Santa Barbara, 93106-3060*
[2]*Department of Geography, University of California, Santa Barbara, 93106-4060*
[3]*NOAA Environmental Technology Laboratory, Boulder, Colorado*

The performance of a network of five CODAR (Coastal Ocean Dynamics Application Radar) high frequency (HF) radars is described based on comparisons with an array of nine moorings in the Santa Barbara Channel and Santa Maria Basin deployed between June 1997 and November 1999. Eight of the moorings carried vector measuring current meters (VMCM's), the ninth an upward-looking acoustic Doppler current profiler (ADCP). Measurement depths were ~1 m for the HF radars, 5 m for the VMCM's, and 3.2 m for the ADCP bin nearest to the surface. Comparison of radial components of near-surface currents from 18 HF radar-mooring pairs yielded root mean square (rms) speed differences of 7-19 cm s^{-1}. The radial components were significantly correlated with r^2 in the range 0.39-0.77. Other studies based on radar-mooring comparisons have found similar rms speed differences and r^2 based on total velocity vectors. Spectral analysis showed significant coherence for frequencies below 2.3 cycles day^{-1} (periods longer than 11 hr). At higher frequencies no significant coherence was found. Comparisons revealed bearing errors in locating radial currents on the sea surface by some of the HF radars. These were typically 5-10^o with a maximum error of 19^o. The effects of bearing errors on total velocity vector estimates were evaluated using a simple flow field and measured bearing errors, showing up to 15% differences in computed flow speeds, and up to ~9^o differences in flow directions.

1. INTRODUCTION

We installed the first HF radar at Coal Oil Point (COP) in June 1997, followed by Pt. Conception (PTC) in August 1997, then Refugio (RFG) in October 1997 (Fig. 1). The fourth and fifth were installed in November 1998 at Pt. Arguello (ARG) and Fallback 22 (FBK) near Pt. Sal. Antennas were placed as close to the ocean as possible to minimize signal attenuation by propagation over land. Each radar transmitted at a different frequency in the range 12.2 - 13.6 megahertz .

The coverage area of the HF radar array included eight moorings deployed in the western Santa Barbara Channel and Santa Maria Basin (open circles, Fig. 1) from 1993 to 1999 by CCS/SIO. Time lines of mooring and HF radar data used for comparison are shown in Fig. 2. The CCS/SIO moorings carried vector measuring current meters (Weller and Davis 1980) at 5 and 45 meters depth providing hourly averages of current velocity. We use the 5 m data for comparison with the surface HF radar data.

An additional mooring, designated ADCP in Figures 1 and 2, was deployed by UCSB investigators near the center of the Santa Barbara Channel from 20 May 1998 to 12

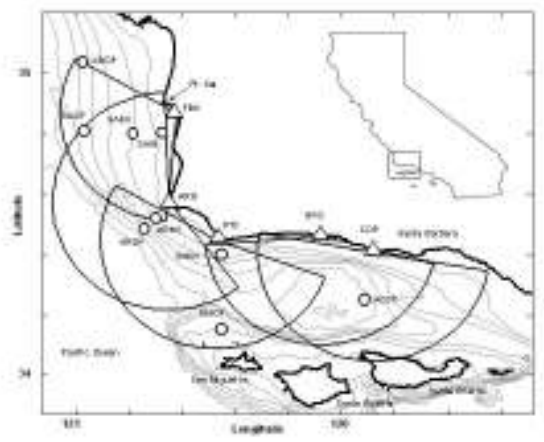

Figure 1. Locations of HF radars are indicated with triangles: Fallback-22 near Pt. Sal (FBK), Pt. Arguello (ARG), Pt. Conception (PTC), Refugio Beach (RFG), and Coal Oil Point (COP). Circular sectors show nominal radar ranges of 42 km. Circles indicate locations of moored current meters used for comparison with HF radar currents. The inset shows the study site relative to the California coast. Bathymetric contours at 50, 100, 200, 300, 400, 500 and 600 m depth are also shown.

October 1999. The UCSB mooring carried an upward looking 1200 kHz acoustic Doppler current profiler (ADCP; manufactured by R.D. Instruments, San Diego CA) at 15 meters depth. The ADCP measured currents over 0.5 m depth increments (bins) to within 3-4 meters of the sea surface, every 20 minutes. These data were subsequently averaged into 1 hr blocks. We compared HF radar time series with the time series from the ADCP bin nominally at 3.2 m depth. This was the shallowest bin consistently free from contamination due to surface reflections.

An overall indicator of radar performance is spatial coverage over time. Coverage is defined as the number of sectors returning radials each hour (Fig. 2b-f). Some moorings were near, or just beyond, the range limits of the radars (42 km), or near the edge of angular coverage range (e.g. ABOF in Fig. 1). An increase in coverage at ARG in November 1999, after the comparison period, resulted from antenna and cable replacement. Causes of coverage variability include power outages, antenna collapse, or other hardware failures. Coverage variations may also result from changing noise sources or variations in the environment around the radar antennas.

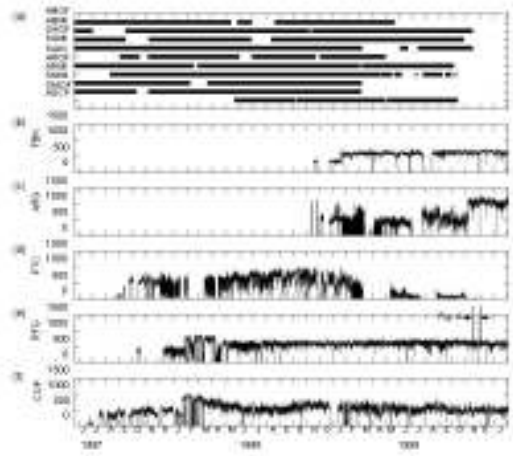

Figure 2. (a) Time lines of the moored current time series used for comparison with the HF radar time series. (b-f) Time series of coverage defined as the number of sectors returning data each hour for the five HF radars. Vertical bars toward the end of the RFG time series denote the two week segment of Fig. 3.

A total of 18 paired mooring-HF radar time series were available with maximum record lengths exceeding one year (Fig. 2). We compared radial components with moored current meters to evaluate performance of individual radars. To examine performance of individual HF radars, we computed various statistics for each pair of HF radar and mooring time series. The square of the correlation coefficient (r^2) was computed between Vm and VHF for the sector containing the mooring, and for sectors surrounding the mooring. Typically, a single radar sector entirely contained the mooring watch circle (50 m to 300 m in radius depending on water depth for the CCS/SIO moorings; 750 m for the ADCP mooring).

2. COMPARISON RESULTS

2.1. Correlation and radial velocity differences

Time series of V_{HF} and V_m typically showed strong tidal variations as in the 2-week example from FBK-SAMI (Fig. 3a). The time series were clearly similar and exhibited significant correlation for this short interval (r2 =0.81, N =314; Fig. 3b). Table 1 summarizes the statistical comparisons between V_{HF} and V_m for all HF radar-mooring pairs over much longer time scales. Values of r^2 fell in the range 0.39-0.77, and root-mean-square (rms) speed difference ranged from 7-19 cm s^{-1}. Biases were typically less than 2 cm s^{-1}, with a maximum of 6 cm s^{-1}. Slopes m of regression lines, defined such that $V_{HF} = V_m \cdot m + b$, were in the range 0.31-0.88 with intercepts b in the range 4.5-8.4 cm s^{-1}.

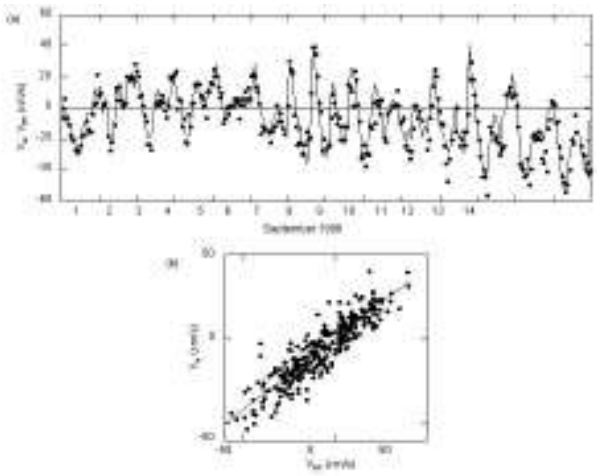

Figure 3. (a) Time series of radial currents V_m from mooring SAMI (solid line) and radial currents V_{HF} from the FBK radar (dots) for 1-14 September 1999. (b) Scatter plot of V_m versus V_{HF} in panel (a). V_m and V_{HF} are significantly correlated with r^2 = 0.81, N = 314 and are related such that V_{HF} = 0.846 V_m+0.535.

Table 1. Summary of Statistical Results

1) Record ranged from 125 hr - 10,186 hrs

2) r^2 ranged from 0.4 to 0.75

3) rms difference ranged from 7 to 19 cm s^{-1}

2.2. Spectral analysis

Power spectra of VHF and Vm were computed for subsets of the time series of Fig. 2 to compare variance levels over time scales of 2 hours to ~20 days. Subsets were chosen to avoid large data gaps occasionally lasting over a month (Fig. 2). For each subset of data, up to 30% of data were missing, and these were filled with zeroes. Representative power spectra for three HF radar-moorings pairs are shown in Fig. 4. Spectral levels generally agreed for frequencies less than 2.3 cycles day-1 (cpd), but levels of VHF tended to be somewhat less than Vm such as for PTC-SMOF in Fig. 4. The diurnal (K1) and semidiurnal (M2) tidal peaks in Vm and VHF were well resolved for FBK-SAOF and PTC-SMOF, and SMIN, but not for the ARG radar. Shoulders in the FBK-SAOF spectra suggest a poorly resolved peak near the inertial frequency (1.13 cpd). Above ~2.2 cpd VHF spectra become nearly white and depart sharply from Vm spectra. At these frequencies Vm spectra have slopes in the range -3 to -2. Noise levels were estimated by computing the mean spectral levels between 7-12 cpd. Assuming these values represent the white noise levels present at all frequencies, they account for ~20% (FBK-SAOF), 15% (PTC-SMOF) and 30% (ARG-SMIN) of variance in spectra shown in Fig. 5, or about 5 - 8 cm s-1 rms.

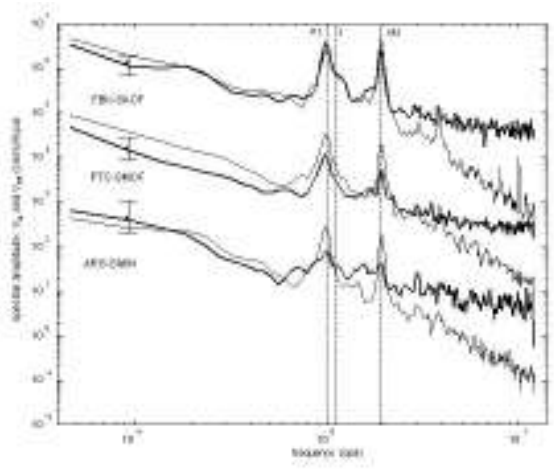

Figure 4. Pairs of power spectra of radial vector time series from three HF radars (bold lines) and three moorings (light lines). From top to bottom radar-mooring pairs are FBK-SAOF, PTC-SMOF, and ARG-SMIN. Vertical lines denote the K1 and M2 tidal frequencies, and f indicates the inertial frequency. The upper two pairs of spectra are offset vertically by factors of 10^2 and 10^4, respectively.

Squared coherence spectra γ^2 were computed between several time series of VHF and Vm to examine correlation versus frequency; the envelope of these spectra is indicated by shading in Fig. 5a. Spectra of γ^2 were averaged together to produce mean γ^2 as an overall measure of coherence versus frequency (bold line, Fig. 5a). The standard deviation σ at each frequency was computed as a measure of variability in γ^2 (thin solid lines indicate mean γ^2 in Fig. 5a). Mean γ^2 fell in the range 0.3-0.7 up to frequencies of about 2.3 cpd where it dropped below the threshold labeled 95%. The threshold was defined such that γ^2 between two unrelated time series would exceed this level only 5 times out of 100. This result indicates significant coherence between Vm and VHF for frequencies less than ~2.3 cpd, the same frequency range over which their power spectra agree (Fig. 5). The phase spectrum was nearly zero over this range and became highly variable at frequencies where mean γ^2 was not significant (Fig. 5b).

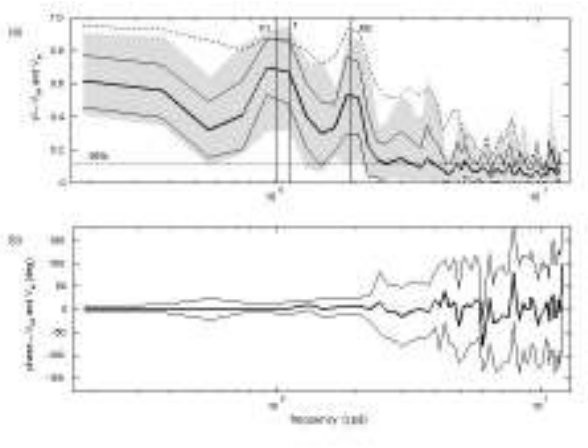

Figure 5. (a) Mean squared coherence spectrum γ^2 between radial currents obtained from the radars V_{HF} and radial currents obtained from the moorings V_m (bold line). Time series used in computing γ^2 are indicated in column 2 of Table 1 by superscript 1. $\gamma^2 \pm$ 1 standard deviation are shown (thin lines) along with envelope of all γ^2 spectra (shading). γ^2 between radial currents measured by the acoustic Doppler profiler at 3.2 m and 8.2 m depth is also shown (dashed line). Vertical lines indicate the K1 and M2 tidal frequencies, and f the inertial frequency. Dotted line shows threshold for significance at 95% confidence level. (b) Mean phase spectrum (bold line) $\pm$1 standard deviation (thin lines) between V_{HF} and V_m.

To investigate how vertical shear near the surface might the affect coherence between V_{HF} and V_m, we computed γ^2 between ADCP time series at 3.2 m and 8.2 m depths (dashed line, Fig. 5a). This depth difference is comparable to the difference in measurement depths of the radars and VMCM's. The rms difference between the ADCP time series at these depths was 5 cm s-1 over the 12,048 hr deployment period. The γ^2 spectrum for the ADCP over this depth range was higher than mean γ^2 for V_m and V_{HF}, but had a somewhat similar shape.

2.3. Bearing offsets

The sector with the highest r2 between V_{HF} and V_m often did not contain the mooring where V_m was measured, but was displaced in bearing. This displacement suggests errors in the radar's determination of direction to sectors on

the ocean's surface. A similar result was reported by (Kosro et al. 1997) from an OSCR system. We argue that in the absence of directional errors, the highest r^2 will coincide with the sector containing the mooring. A broad peak in r^2 may occur if the spatial correlation scales of the velocity field are large in the azimuthal and radial directions. We define the displacement in bearing, or bearing offset $\Delta\theta$ as,

$$\Delta\theta = \theta_r - \theta_m, \qquad (2)$$

where θ_r is the bearing to center of the sector with maximum r^2, and θ_m is the bearing to the mooring. Positive $\Delta\theta$ indicates that the sector with maximum r^2 is displaced clockwise from the mooring. $\Delta\theta$ ranged from –16° to 19° with an average absolute value of 7°, although $\Delta\theta$ could only be determined to within the 5° sector width

An example of a large bearing offset, $\Delta\theta$ = -16°, was found for PTC-SMIN (Fig. 6). The maximum in r^2 was broad, but its peak was clearly offset from SMIN as indicated by r^2 profiles along constant range lines of 4.5, 6.0, and 7.5 km (Fig. 7). The maximum r^2 occurred in the same 1.5 km range cell as SMIN, such that the offset was in bearing only. A small bearing offset was found for COP-ADCP with $\Delta\theta$ = -1° (Figure 8). Here the sector with maximum r2 contained the mooring location and a broad maximum extended over bearing and range (Figure 9).

Figure 10 shows how $\Delta\theta$ changed with bearing for the PTC, ARG, and FBK radars. Each of these radars had more than one mooring within their coverage areas. At PTC, with four moorings in its coverage area, $\Delta\theta$ increased roughly monotonically with bearing from $\Delta\theta$ = –15° at bearing 160° to $\Delta\theta$ = 9 ° at 291° (open squares, Fig. 10). Values of $\Delta\theta$ were only determined near the end points of this range, however. At ARG, $\Delta\theta$ also increased with bearing up to a maximum of $\Delta\theta$ = 19° at 311° followed by a decrease to $\Delta\theta$ = 10° at 355°. At FBK, $\Delta\theta$ reached a minimum of –11° at 216° then increased to 16° at 299°.

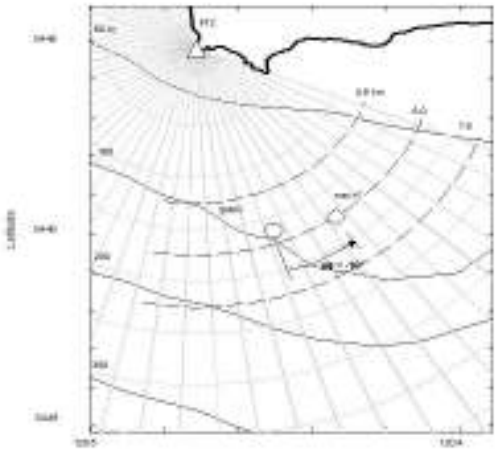

Figure 6. (a) Location of Point Conception radar PTC (triangle) and mooring SMIN (circle). Radial current vectors V_{HF} were found for sectors 1.5 km in radius by 5° in azimuth (gray lines). Radial currents V_m were measured in situ at the mooring. The diamond indicates the sector with the highest r^2 between V_{HF} and V_m. The arrow shows bearing offset $\Delta\theta$ between the mooring location and the sector with highest r^2. Dashed arcs show the locations of r^2 profiles plotted in Fig. 7 (a), (b), and (c).

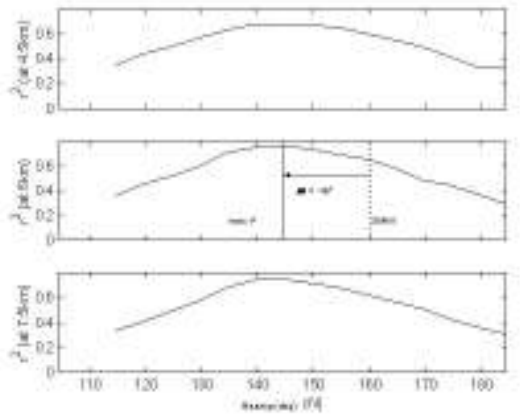

Figure. 7. Profiles of r^2 between V_{HF} and V_m from PTC and SMIN are shown along ranges of (a) 4.5 km, (b) 6.0 km, and (c) 7.5 km. Bearing to SMIN location is designated with a dashed line, with the maximum r^2 shown with a solid line.

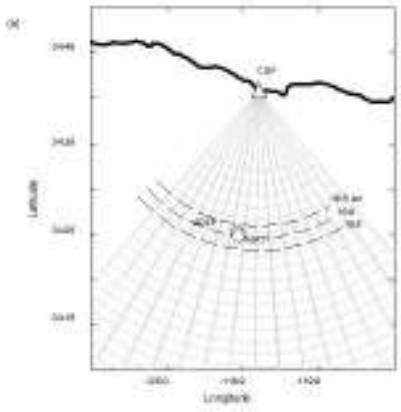

Figure 8. (a) As in Fig. 7, but for the Coal Oil Point radar COP and mooring ADCP.

We measured antenna patterns at PTC, RFG, and COP by moving a transponder in a small boat along circular arcs within the coverage areas of the radars. Antenna patterns from these sites exhibited varying levels of distortion (data not shown). Antenna patterns measured at RFG and PTC were typical of patterns found elsewhere, while patterns at COP were moderately distorted.

In principle, antenna pattern distortions can be accounted for in the MUSIC algorithm, and techniques for

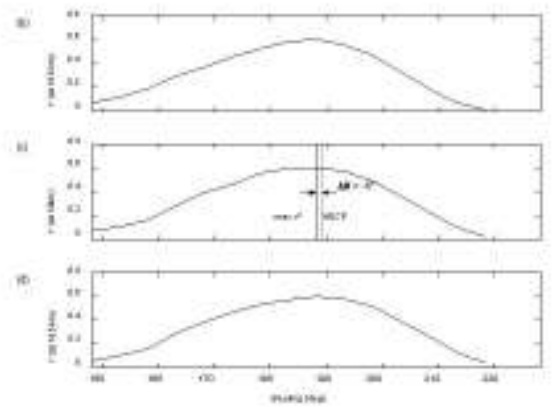

Figure 9. Profiles of r^2 between V_{HF} and V_m are shown along ranges of (a) 16.5 km, (b) 18.0 km, and (c) 19.5 km.

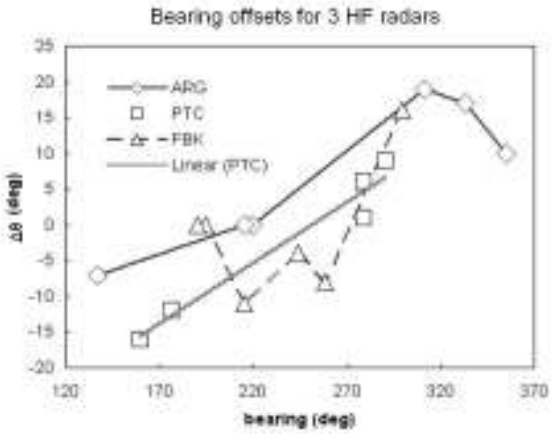

Figure 10. Bearing offset $\Delta\theta$ versus bearing for all radars with more than one mooring in coverage areas: Point Conception (PTC, squares, gray line is a linear least square fit), Point Arguello (ARG, diamonds, solid black line), and Fallback-22 (FBK, triangles, dashed line).

doing so are in development (e.g. (Barrick and Lipa 1999)). During the data collection phase of this study, corrections for antenna pattern distortion were unavailable, and HF data used to compute $\Delta\theta$ assumed ideal antenna patterns. We compared observations of $\Delta\theta$ with measured antenna patterns to look for a direct relationship between distortions in the measured patterns and non-zero values of $\Delta\theta$. For example, following a suggestion by J. Paduan (personal communication, 2000), a relationship between $\Delta\theta$ and the rate of change of the measured antenna responses versus bearing was investigated. Extensive experimentation failed to reveal a consistent relationship between $\Delta\theta$ and measured antenna patterns. When procedures for incorporating measured antenna patterns into estimates of V_{HF} are available, we intend to test them by mapping r^2 around moorings as in figures 6 and 8. We hypothesize that accounting for antenna pattern distortions would result in lower $\Delta\theta$.

Another factor affecting $\Delta\theta$ is phase calibration of the three-element receive antenna. Each element responds to incoming signals with differing voltage phase depending on signal direction. Phase calibrations were initially determined at PTC from sea echo as part of the CODAR data processing procedures (Barrick and Lipa 1986). Later, phases were directly measured with the transponder during the antenna pattern measurements and used in processing. We computed $\Delta\theta$ between PTC and SMIN for each of these time periods to test the effect of phase settings. Using sea echo phases resulted in $\Delta\theta \sim 30^o$, while transponder phases resulted in $\Delta\theta \sim 15^o$, as shown in Fig. 11, which shows how $\Delta\theta$ varied as a function of time. The reduction in $\Delta\theta$ using the transponder phase suggests a strong link between receive antenna characteristics and $\Delta\theta$.

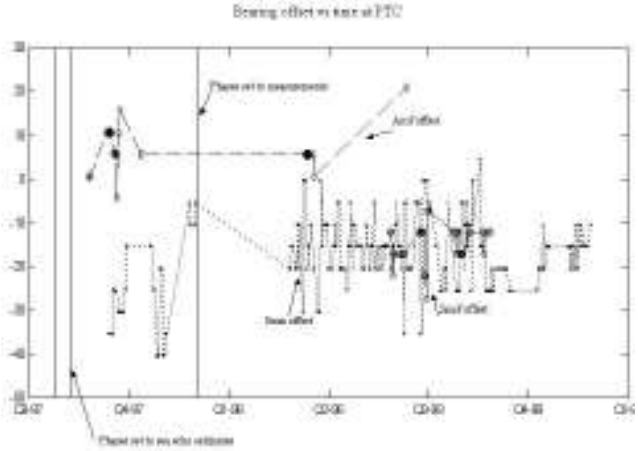

Figure 11. Bearing offset $\Delta\theta$ for PTC-SMIN (dotted line, black dots), PTC-SMOF (solid line, circles), and PTC-AROF (dashed lin, diamonds), as a function of time. Each data point is computed from a 2-week moving window. Vertical lines show time phases were set to those computed from sea-echo and transponder measurements.

2.4. Effect of Δθ

Bearing offsets $\Delta\theta$ in HF radial data ultimately produce errors in total velocity vectors determined from two or more radars. We examined effects of variable $\Delta\theta$ on total velocity vectors by simulating its effect on an idealized flow field. For simplicity, we used a uniform westward flow along a straight coast (black arrows, Fig. 12). Patterns of V_{HF} as functions of range and bearing were computed at two sites labeled A and B in Fig. 12. At site A, bearings to sectors on the sea surface were distorted by $\Delta\theta$ using the slope of the linear least square fit for the PTC radar (gray straight line, Fig. 10): over bearings 90^o-270^o, $\Delta\theta$ in the range -18^o to 14^o were added to the bearing. Total velocity vectors (black arrows, Fig. 12) were computed on a 2km grid, from V_{HF} at sites A and B. Following the method of (Gurgel 1994), a total velocity vector at each grid point

was computed from all V_{HF} within a circle (3 km radius) centered on the grid point. A similar procedure was used by (Paduan and Rosenfeld 1996). The mean difference in flow speeds between the original vectors (black arrows, Fig. 12) and distorted vectors (gray arrows, Fig. 12) was ~7% of the original uniform flow speed with a maximum difference of ~15%. The mean difference in flow direction was ~2.5°, with a maximum of ~9°. Simulations with other simple flow fields produced comparable errors in total velocities (results not shown). These errors are significant and reinforce the need for incorporation of antenna pattern corrections in the direction finding algorithms used with these radar systems.

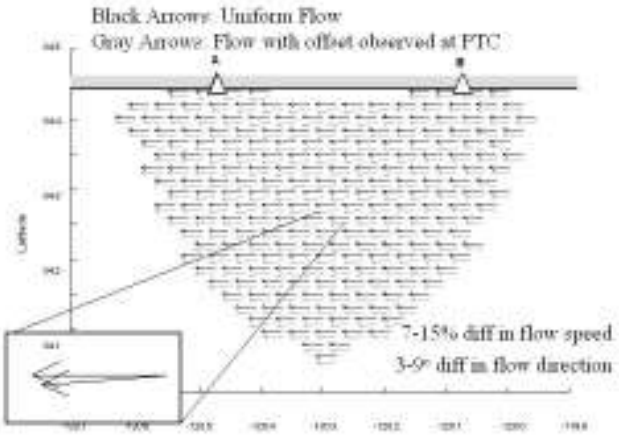

Figure 12. Black arrows (offset for clarity) show uniform westward flow parallel to a straight coastline (bold line and shading) used for modeling effects of bearing offset $\Delta\theta$ on total velocity vectors. Arrows are placed on grid with 4 km spacing. Gray arrows show total vectors computed from radar sites located at A and B (triangles). Radial currents V_{HF} measured at A were distorted with the observed bearing offset $\Delta\theta$ at PTC as explained in text.

3. CONCLUSIONS

We compared radial components of near-surface ocean currents (radials) from 18 pairs of moored current meters and five HF radars (transmitting at frequencies of 12-13 Mhz) from the Santa Barbara Channel and Santa Maria Basins. Comparisons were based on observations between June 1997 and November 1999 with record lengths of 5 to 424 days. Eight vector measuring current meters moored at 5 m depth and one acoustic Doppler current profiler with its shallowest bin at 3.2 m were compared with HF radar currents at ~ 1 m. Our analysis supports the following conclusions:

1. Radials obtained from the radars were significantly correlated with radials obtained from the moored current meters with r^2 in the range 0.39-0.77. Root-mean-square (rms) radial speed differences ranged from 7-19 cm s^{-1}. A weak trend of increasing rms differences was found with increasing range.

2. Significant coherence was found between current meter and radar-derived time series for frequencies below 2.2 cpd (11 hour period and longer). Power spectra show similar magnitudes and slopes for frequencies below 2.2 cpd.

3. A pointing error $\Delta\theta$ ranging from -16^o to19^o was found for some of the radar sites where positive values indicate a clockwise error. $\Delta\theta$ for a given radar was not constant, but varied with bearing. We speculate that $\Delta\theta$ resulted from distortions of the receive antenna patterns in the near field.

4. We used a simple model of $\Delta\theta$ versus bearing based on our observations to simulate errors in total velocity vectors computed from two radars. Using a uniform flow parallel to shore, $\Delta\theta$ produced speed errors of up 15% and direction errors up to 9° in total velocity vectors.

Acknowledgements. This research was supported by the Minerals, Management Service, U.S. Department of the Interior, MMS Agreement 14-35-0001-30758. Support was also provided by the W.M. Keck foundation and the David and Lucile Packard Foundation, as part of the Partnership for Interdisciplinary Studies of Coastal Oceans (PISCO). The views and conclusions contained in this document are those of the authors and should not be interpreted as necessarily representing the official policies, either express or implied, of the U.S. Government.

REFERENCES

Barrick, D.E., 1980: Accuracy of parameter extraction from sample-averaged sea-echo Doppler spectra. *IEEE Transactions on Antennas and Propagation*, 28 (1), 1-11.

Barrick, D.E., and B.J. Lipa, 1986: Correcting for Distorted Antenna Patterns in CODAR Ocean Surface Measurements. *IEEE Journal of Oceanic Engineering*, OE-11 (2), 304-309.

Barrick, D.E., and B.J. Lipa, 1997: Evolution of bearing determination in HF current mapping radars. *Oceanography*, 10 (2), 72-75.

Barrick, D.E., and B.J. Lipa, 1999: Using antenna patterns to improve the quality of SeaSonde HF radar surface current maps. *IEEE 6th Working Conference on Current Measurement*.

Bendat, J.S., and A.G. Piersol, *Random Data analysis and measurement procedures*, 566 pp., Wiley-Interscience, New York, 2000.

Chapman, R.D., and H.C. Graber, 1997: Validation of HF radar measurements. *Oceanography*, 10 (2), 76-79.

Chapman, R.D., L.K. Shay, H.C. Graber, J.B. Edson, A. Karachintsev, C.L. Trump, and D.B. Ross, 1997: On the accuracy of HF radar surface current measurements: Intercomparison with ship-based sensors. *Journal of Geophysical Research*, 102 (C8), 18,737-18,748.

Crombie, D.D., 1955: Doppler Spectrum of Sea Echo at 13.56 Mc/s. *Nature*, 175, 681-682.

Davies, K., 1990: *Ionospheric Radio*. IEEE Electromagnetic Waves Series, 31.

Dorman, C.E., and C.D. Winant, 2000: The Structure and Variability of the Marine Atmosphere around the Santa Barbara Channel. *Monthly Weather Review*, 128, 261-282.

Georges, T.M., 1980: Progress toward a practical skywave sea-state radar. *IEEE Trans. Antennas Propagat*., 28 (6), 751-761.

Graber, H.C., B.K. Haus, R.D. Chapman, and L.K. Shay, 1997: HF radar comparison with moored estimates of current speed and direction: Expected differences and implications. *Journal of Geophysical Research*, 102 (C8), 18,749-18,766.

Gurgel, K.W., 1994: Shipborne measurement of surface current fields by HF radar. *L'Onde Electrique*, 74 (5), 54-59.

Harlan, J.A., S.E. Swearer, R.R. Leben, and C.A. Fox, 2000: Surface Circulation in a Caribbean Island Wake. (in review).

Harms, S., and C.D. Winant, 1998: Characteristic patterns of the circulation in the Santa Barbara Channel. *Journal of Geophysical Research*, 103 (C2), 3041-3065.

Kosro, P.M., 1987: Structure of the coastal current field off northern california during the coastal ocean dynamics experiment. *Journal of Geophysical Research*, 92 (c2), 1637-1654.

Kosro, P.M., J.A. Barth, and T.P. Strub, 1997: The coastal jet: Observations of surface currents over the Oregon continental shelf from HF radar. *Oceanography*, 10 (2), 53-57.

Kraus, J.D., *Antennas*, McGraw-Hill, 1988.

Laws, K.E., D.M. Fernandez, and J.D. Paduan, 2000: Simulation-based evaluations of HF radar ocean current algorithms. *Journal of Atmospheric and Oceanic Technology*, submitted.

Melton, D.C., 1995: Remote sensing and validation of surface currents from HF radar. M.S. Thesis, Naval Postgraduate School, 66pp.

Paduan, J.D., and L.K. Rosenfeld, 1996: Remotely sensed surface currents in Monterey Bay from shore-based HF radar (Coastal Ocean Dynamics Application Radar). *Journal of Geophysical Research*, 101 (C9), 20,669-20,686.

Prandle, D., S.G. Loch, and R. Player, 1993: Tidal flows through the Straits of Dover. *Journal of Physical Oceanography*, 23,, 23-37.

Schmidt, R.O., 1986: Multiple Emitter Location and Signal Parameter Estimation. *IEEE Transactions on antennas and propagation*, AP-34 (3), 276-280.

Shay, L.K., H.C. Graber, D.B. Ross, and R.D. Chapman, 1995: Mesoscale ocean surface current structure detected by high-frequency radar. *Journal of Atmospheric and Oceanic Technology*, 12, 881-900.

Shay, L.K., S.J. Lentz, H.C. Graber, and B.K. Haus, 1998: Current structure variations detected by high-frequency radar and vector-measuring current meters. *Journal of Atmospheric and Oceanic Technology*, 15, 237-256.

Stewart, R.H., and J.W. Joy, 1974: HF radio measurements of surface currents. *Deep Sea Research*, 21, 1039-1049.

Vesecky, J., C. Teague, D. Fernandez, J. Paduan, J. Daida, R. Onstott, K. Laws, and P. Hansen, 1998: Coastal Currents with HF radar. *Backscatter*, 13, 12-20.

Weller, R.A., and R.E. Davis, 1980: A vector measuring current meter. *Deep-Sea Research*, 27, 565-582.

Brian M. Emery, ICESS, 6831 Ellison Hall, Univ. of California, Santa Barbara CA, 93106

Jack A. Harlan, NOAA Environmental Technology Laboratory 325 Broadway, Boulder, CO 80305

Libe Washburn, ICESS, 6831 Ellison Hall, Univ. of California, Santa Barbara CA, 93106